Noname manuscript No.
(will be inserted by the editor)

High-speed Dynamic Gait Generation for Limit Cycle Walkers Based on Forward-tilting Impact Posture

Fumihiko Asano

Received: date / Accepted: date

Abstract This paper proposes a novel method for generating a dynamic gait based on anterior-posterior asymmetric impact posture tilting the robot's center of mass forward. The primary purpose of this method is to asymmetrize the impact posture by actuating the robot's telescopic-legs to make overcoming the potential barrier at mid-stance easy, and the mechanical energy is accordingly restored. First, we introduce a planar rimless wheel model with telescopic legs, and investigate the validity of the stance-leg extension control. The basic properties and efficiency of the generated gait are also numerically analyzed. Second, we extend the method to a planar telescopic-legged biped model, and investigate the validity through numerical simulations. We also discuss the role of asymmetric shape of human foot from the brake effect point of view through efficiency analysis taking the ankle-joint actuation into account.

Keywords Limit cycle walking · Impact posture · Potential barrier

1 Introduction

Limit cycle walkers including McGeer's passive-dynamic bipeds [1] can generate natural and energy-efficient dynamic gaits utilizing their own physical dynamics and passivity. By applying a suitable actuation rule to the robot, efficient level walking can be achieved [2][3][4][5], however, guaranteeing the limit cycle stability is another problem and is not easy.

One of the most impeditive problems in stable limit cycle generation is the potential barrier at mid-stance where the robot's potential energy is maximized. The robot must start walking with a suitable and sufficient initial

F. Asano
School of Information Science, Japan Advanced Institute of Science and Technology
1-1 Asahidai, Nomi, Ishikawa 923-1292, Japan
Tel.: +81-761-51-1243
Fax: +81-761-51-1149
E-mail: fasano@jaist.ac.jp

momentum to overcome the potential barrier and to reach the next impact. It is not easy to guarantee overcoming the potential barrier only with intuitive control laws in limit cycle walking. It is also difficult to start walking from a standing posture smoothly and we must search the suitable initial conditions through a trial and error process.

The potential barrier in dynamic gait originally comes from the fact that most limit cycle walkers have anterior-posterior symmetric impact posture as shown in Fig. 1 (a). A compass-like biped robot [2], for example, must maintain symmetric posture involuntary, and this creates the potential barrier at mid-stance. If the robot can create asymmetric impact posture tilting forward as shown in Fig. 1 (b), this problem can be solved. The easiest way to asymmetrize the impact posture is to lengthen the stance leg during stance phases using the prismatic joint while shortening the swing leg. The importance of forward-tilting impact posture has also been discussed in several related works [6][7][8].

On the other hand, the author has wondered about the meaning of anterior-posterior asymmetry of human foot. As the authors have shown, such as in virtual passive dynamic walking, fully-actuated limit cycle walkers must avoid negative actuator work at every joint for achieving energy-efficient walking [4]. This results in that the rotary actuator at the stance ankle must continue forward driving of the stance leg without braking. We assumed that, however, the stance leg is always rotating forward. The zero moment point (ZMP) is then shifted posterior to the ankle joint. This implies that, in robot foot, the heel-side must be longer than the toe-side. Human foot is, however, formed of inverse shape and this implies that it can drive the stance leg backward only. In other words, human foot is not suitable to drive the body or the stance leg forward. It is thus believed that humans walk forward while putting on the ankle brake. This understanding, however, conflicts efficient limit-cycle walkers. Exploring this question is another subject of our study.

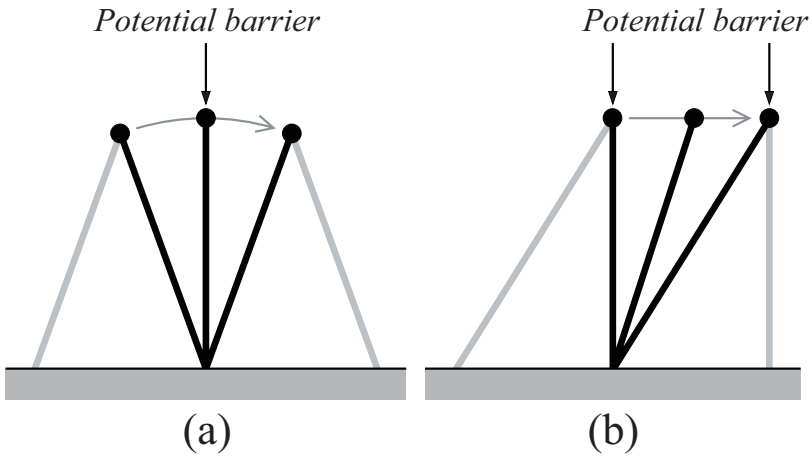

Fig. 1 Relations between impact posture and potential barrier

Based on the observations, in this paper, we propose a novel method for generating a level dynamic gait by asymmetrizing the impact posture using the telescopic-leg's action. The primary purpose of this method is to tilt or shift the robot's center of mass (CoM) forward for overcoming the potential barrier at mid-stance easy, and the mechanical energy is accordingly restored. First, we introduce a planar rimless wheel model that consists of eight telescopic legs, and investigate the validity of the proposed method. Second, we extend the method to a planar telescopic-legged biped robot with flat feet incorporating a brake spring and numerically investigate the gait descriptors, especially the behavior of ZMP. Through numerical simulations, we discuss the anterior-posterior asymmetry of human foot from the ZMP point of view.

This paper is organized as follows. Section 2 investigates the validity of the method using a simple rimless wheel model with telescopic legs. Section 3 extends the method to a planar telescopic-legged biped model with flat feet and ankle brake. Finally, section 4 concludes this paper and describes the future research directions.

2 Dynamic Gait Generation of Telescopic-legged Rimless Wheel

2.1 Modeling of telescopic-legged rimless wheel

2.1.1 Dynamic equation

Fig. 2 shows the model of a planar telescopic-legged rimless wheel (TRW). We call the leg frame on the floor "stance leg", and assume that only the stance leg is actuated and other legs are kept l_0 [m]. We also assume that this model has a point mass, M [kg], concentrated on the central position and the inertia moment about the CoM can be neglected. In this paper, we set $\alpha = \pi/4$ [rad], i.e. eight legged, and $l_0 = 1.0$ [m].

Fig. 3 shows the essential part of the TRW which determines the stance-phase motion. This is just a variable length pendulum and its dynamic equation becomes very simple. Let $\boldsymbol{q} = \begin{bmatrix} \theta & l \end{bmatrix}^{\mathrm{T}}$ be the generalized coordinate vector, the dynamic equation of the TRW then becomes

$$\boldsymbol{M}(\boldsymbol{q})\ddot{\boldsymbol{q}} + \boldsymbol{h}(\boldsymbol{q}, \dot{\boldsymbol{q}}) = \boldsymbol{S}u, \tag{1}$$

where

$$\boldsymbol{M}(\boldsymbol{q}) = \begin{bmatrix} Ml^2 & 0 \\ 0 & M \end{bmatrix},$$
$$\boldsymbol{h}(\boldsymbol{q}, \dot{\boldsymbol{q}}) = \begin{bmatrix} 2Ml\dot{l}\dot{\theta} - Mlg\sin\theta \\ -Ml\dot{\theta}^2 + Mg\cos\theta \end{bmatrix},$$
$$\boldsymbol{S} = \begin{bmatrix} 0 \\ 1 \end{bmatrix} u,$$

and u [N] is the control force of the linear actuator to extend/retract the telescopic-leg frame.

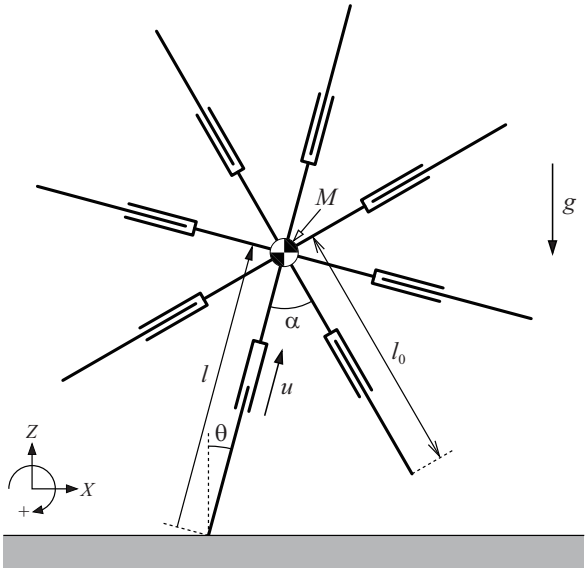

Fig. 2 Model of planar telescopic-legged rimless wheel

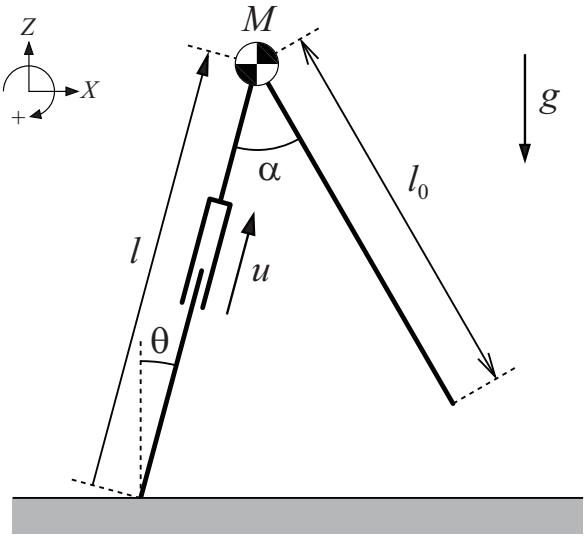

Fig. 3 Essential part of telescopic-legged rimless wheel

2.1.2 Transition equations and energy-loss coefficient

Fig. 4 shows the configuration of impact phase. From this figure, the relations of the angular position and the stance-leg length can be found to be

$$\theta^+ = \theta^- - \alpha, \tag{2}$$

$$l^+ = l_0. \tag{3}$$

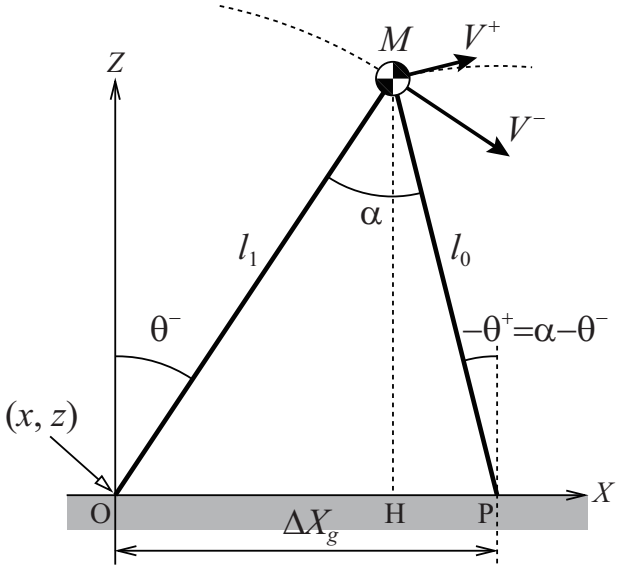

Fig. 4 Asymmetric impact posture

The point H in this figure is the ground projection of the CoM, X_g, and ΔX_g is the step length which is identical to the distance X_g moved during one step.

The following derives the transition equations of the velocities. We introduce an extended coordinate vector $\bar{\boldsymbol{q}} = \begin{bmatrix} x & z & \theta \end{bmatrix}^{\mathrm{T}}$ where (x, z) is the stance-leg's tip position. The inelastic collision is then modeled as

$$\bar{\boldsymbol{M}}(\theta)\dot{\bar{\boldsymbol{q}}}^+ = \bar{\boldsymbol{M}}(\theta)\dot{\bar{\boldsymbol{q}}}^- - \boldsymbol{J}_I(\theta)^{\mathrm{T}}\boldsymbol{\lambda}_I, \tag{4}$$

$$\boldsymbol{J}_I(\theta)\dot{\bar{\boldsymbol{q}}}^+ = \boldsymbol{0}_{2\times 1}, \tag{5}$$

where $\bar{\boldsymbol{M}}(\theta) \in \mathbb{R}^{3\times 3}$ is detailed as

$$\bar{\boldsymbol{M}}(\theta) = \begin{bmatrix} M & 0 & Ml_1\cos\theta \\ 0 & M & -Ml_1\sin\theta \\ Ml_1\cos\theta & -Ml_1\sin\theta & Ml_1^2 \end{bmatrix}. \tag{6}$$

Note that θ in this case is not that in $\boldsymbol{q}$ but that in $\bar{\boldsymbol{q}}$, and is equal to θ^- in Fig. 4. The extended coordinate does not take stance-leg exchange into account, that is, $\bar{\boldsymbol{q}}^- = \bar{\boldsymbol{q}}^+$ and $\theta^- = \theta^+$ hold in this system. We must reset θ^+ for $\boldsymbol{q}$ following Eq. (2) after impact.

$\boldsymbol{J}_I(\theta) \in \mathbb{R}^{2\times 3}$ is the Jacobian matrix for inelastic collision. We assume that there is a high friction at the contact point and the leg's end-point does not slide immediately after impact. The conditions for velocity constraint are given by

$$\frac{\mathrm{d}}{\mathrm{d}t}\left(x + l_1\sin\theta + l_0\sin(\alpha-\theta)\right)^+ = 0, \tag{7}$$

$$\frac{\mathrm{d}}{\mathrm{d}t}\left(z + l_1\cos\theta - l_0\cos(\alpha-\theta)\right)^+ = 0. \tag{8}$$

These lead to

$$\dot{x}^+ + l_1\dot{\theta}^+\cos\theta - l_0\dot{\theta}^+\cos(\alpha-\theta) = 0, \tag{9}$$

$$\dot{z}^+ - l_1\dot{\theta}^+\sin\theta - l_0\dot{\theta}^+\sin(\alpha-\theta) = 0. \tag{10}$$

By summarizing these equations, we can formulate $\boldsymbol{J}_I(\theta)$ as

$$\begin{bmatrix}0\\0\end{bmatrix} = \begin{bmatrix}1 & 0 & l_1\cos\theta - l_0\cos(\alpha-\theta)\\ 0 & 1 & -l_1\sin\theta - l_0\sin(\alpha-\theta)\end{bmatrix}\dot{\boldsymbol{q}}^+ =: \boldsymbol{J}_I(\theta)\dot{\boldsymbol{q}}^+. \tag{11}$$

Following Eqs. (4) and (5), the velocity vector immediately after impact is derived as

$$\dot{\boldsymbol{q}}^+ = \left(\boldsymbol{I}_3 - \bar{\boldsymbol{M}}(\theta)^{-1}\boldsymbol{J}_I(\theta)^{\mathrm{T}}\boldsymbol{X}_I(\theta)^{-1}\boldsymbol{J}_I(\theta)\right)\dot{\boldsymbol{q}}^-, \tag{12}$$

$$\boldsymbol{X}_I(\theta) := \boldsymbol{J}_I(\theta)\bar{\boldsymbol{M}}(\theta)^{-1}\boldsymbol{J}_I(\theta)^{\mathrm{T}}, \tag{13}$$

however, the inverse of matrix $\bar{\boldsymbol{M}}(\theta)$ cannot be determined because of $\det(\bar{\boldsymbol{M}}(\theta)) = 0$. To solve this problem, we then derive $\dot{\boldsymbol{q}}^+$ by adding an inertia moment, I [kg·m^2], to the model temporarily. The inertia matrix, $\bar{\boldsymbol{M}}(\theta)$, is then adjusted as

$$\bar{\boldsymbol{M}}(\theta) = \begin{bmatrix} M & 0 & Ml_1\cos\theta \\ 0 & M & -Ml_1\sin\theta \\ Ml_1\cos\theta & -Ml_1\sin\theta & I + Ml_1^2 \end{bmatrix}. \tag{14}$$

The determinant then becomes $\det(\bar{\boldsymbol{M}}(\theta)) = M^2 I$ and $\dot{\boldsymbol{q}}^+$ is derived as

$$\dot{\boldsymbol{q}}^+ = \begin{bmatrix} -l_1\cos\theta + l_0\cos(\theta-\alpha) \\ l_1\sin\theta - l_0\sin(\theta-\alpha) \\ 1 \end{bmatrix}\frac{(I + Ml_0l_1\cos\alpha)\,\dot{\theta}^-}{I + Ml_0^2}. \tag{15}$$

By extracting the third element of $\dot{\boldsymbol{q}}^+$, we get

$$\dot{\theta}^+ = \frac{I + Ml_0l_1\cos\alpha}{I + Ml_0^2}\dot{\theta}^-. \tag{16}$$

We then obtain

$$\lim_{I\to 0}\dot{\theta}^+ = \frac{l_1\cos\alpha}{l_0}\dot{\theta}^-. \tag{17}$$

Further, by setting $l_0 = l_1$, we obtain

$$\dot{\theta}^+ = \dot{\theta}^-\cos\alpha. \tag{18}$$

This equation is the same as that of the rimless wheel [9] and the simplest walking model [10]. On the other hand, from the geometric relation at impact, the relation $l_1\cos\theta = l_0\cos(\alpha-\theta)$ holds and the first element of $\dot{\boldsymbol{q}}^+$ is found to be zero, that is, $\dot{x}^+ = 0$. In addition, $l_1\sin\theta - l_0\sin(\theta-\alpha)$ is identical to the step length, ΔX_g, in Fig. 4, and the second element of $\dot{\boldsymbol{q}}^+$ is thus always positive.

As seen from Fig. 4, the velocity immediately before impact is $V^- = l_1\dot{\theta}^-$ [m/s] and that immediately after impact is $V^+ = l_0\dot{\theta}^+ = l_1\dot{\theta}^-\cos\alpha$ [m].

The kinetic energies immediately before and immediately after impact then becomes

$$K^- = \frac{1}{2}M\left(V^-\right)^2 = \frac{1}{2}M\left(l_1\dot{\theta}^-\right)^2, \tag{19}$$

$$K^+ = \frac{1}{2}M\left(V^+\right)^2 = \frac{1}{2}M\left(l_1\dot{\theta}^-\cos\alpha\right)^2. \tag{20}$$

The energy-loss coefficient then becomes

$$\varepsilon = \frac{K^+}{K^-} = \cos^2\alpha \tag{21}$$

regardless of the ratio of leg length.

In a passive RW, the impact posture is always identical, and both the energy-loss coefficient and the restored mechanical energy are kept constant automatically. It then satisfies the following recurrence formula of kinetic energy immediately before impact:

$$K^-[i+1] = \varepsilon K^-[i] + \Delta E, \tag{22}$$

where i is the number of steps [9]. Asymptotic stability of the generated gait is thus guaranteed under the assumption that the next heel-strike always occurs. In a TRW with asymmetric impact posture, ε becomes always the same, and the convergence speed to the steady motion then becomes constant regardless of the extended leg-length if ΔE can also be kept constant simultaneously. Although ΔE is not constant, the limit cycle stability is very high in terms of convergence speed. This is described later.

2.2 Output following control for stance-leg extension

Let the stance-leg length, $l = \boldsymbol{S}^{\mathrm{T}}\boldsymbol{q}$, be the control output. Its second order time derivative then becomes

$$\ddot{l} = \boldsymbol{S}^{\mathrm{T}}\ddot{\boldsymbol{q}} = \boldsymbol{S}^{\mathrm{T}}\boldsymbol{M}(\boldsymbol{q})^{-1}\left(\boldsymbol{S}u - \boldsymbol{h}(\boldsymbol{q},\dot{\boldsymbol{q}})\right), \tag{23}$$

and we can achieve the input-output linearization by the following control input

$$u = \left(\boldsymbol{S}^{\mathrm{T}}\boldsymbol{M}(\boldsymbol{q})^{-1}\boldsymbol{S}\right)^{-1}\left(\bar{u} + \boldsymbol{S}^{\mathrm{T}}\boldsymbol{M}(\boldsymbol{q})^{-1}\boldsymbol{h}(\boldsymbol{q},\dot{\boldsymbol{q}})\right), \tag{24}$$

which leads to $\ddot{l} = \bar{u}$. We introduce a 5-order time dependent function for the desired trajectory of l, which is specified as follows.

$$l_{\mathrm{d}}(t) = \begin{cases} \sum_{k=0}^{5} a_k t^k & (0 \le t < T_{\mathrm{set}}) \\ l_1 & (t \ge T_{\mathrm{set}}) \end{cases} \tag{25}$$

The boundary conditions are chosen as follows.

$$l_{\mathrm{d}}(0^+) = l_0,\ l_{\mathrm{d}}(T_{\mathrm{set}}) = l_1,\ \dot{l}_{\mathrm{d}}(0^+) = \dot{l}_{\mathrm{d}}(T_{\mathrm{set}}) = 0,\ \ddot{l}_{\mathrm{d}}(0^+) = \ddot{l}_{\mathrm{d}}(T_{\mathrm{set}}) = 0$$

The coefficients are then determined as

$$a_5 = \frac{6(l_1 - l_0)}{T_{\rm set}^5},\ a_4 = \frac{15(l_0 - l_1)}{T_{\rm set}^4},\ a_3 = \frac{10(l_1 - l_0)}{T_{\rm set}^3},\ a_2 = a_1 = 0,\ a_0 = l_0.$$

By setting $\bar{u} = \ddot{l}_{\rm d}$ in Eq. (24), we can achieve $l(t) \equiv l_{\rm d}(t)$.

2.3 Dynamic gait generation from standing posture

We first choose the extended leg length, l_1, as

$$l_1 = \frac{l_0}{\cos\alpha} \tag{26}$$

to make the impact posture rectangular triangle. This is the sufficient condition for overcoming the potential barrier, and is conservative. In this case, following Eqs. (17) and (26), the angular velocity immediately after impact becomes

$$\dot{\theta}^+ = \frac{l_0}{\cos\alpha} \cdot \frac{\cos\alpha}{l_0}\dot{\theta}^- = \dot{\theta}^-. \tag{27}$$

Fig. 5 shows the simulation results where $M = 1.0$ [kg] and $T_{\rm set} = 0.40$ [s]. The TRW started from the initial conditions of $\theta = 0$ [rad], $l = l_0$ [m], $\dot{\theta} = 0.001$ [rad/s], and $\dot{l} = 0$ [m/s]. The control of the stance-leg extension in

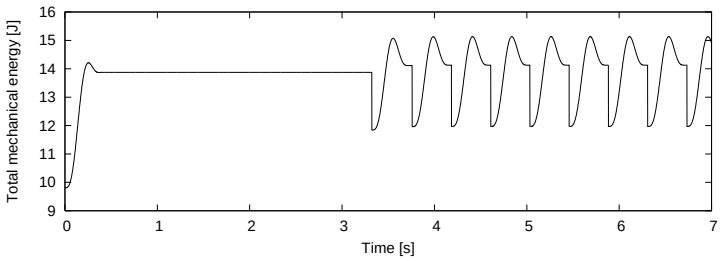

(a) Total mechanical energy

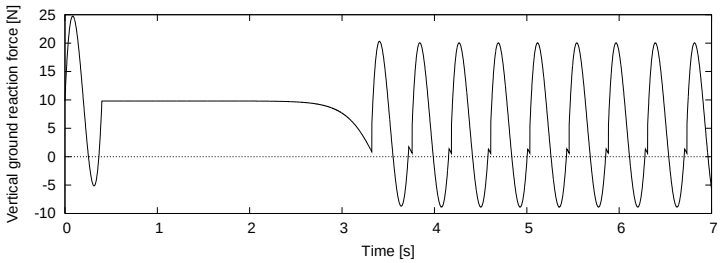

(b) Vertical ground reaction force

Fig. 5 Simulation results of dynamic walking based on asymmetric impact posture where $T_{\rm set} = 0.40$ [s] and $l_1 = \sqrt{2}l_0$ [m]

the first step begins at $t = 0.0$ [s] and is completed at $t = T_{\rm set} = 0.40$ [s]. The mechanical energy is accordingly restored. The angular velocity is, however, still small and the TRW gently falls down as a 1-DOF rigid body keeping the total mechanical energy constant. The first impact occurs at about $t = 3.3$ [s] and the kinetic energy correspondingly dissipates. After several steps, the step period converged to 0.4247 [s]. The walking speed also converged to 2.354 [m/s], and this is remarkable high-speed considering the leg length and the mechanism without having springs nor semicircular feet [11].

From Fig. 5 (b), however, we can see that the vertical ground reaction force (GRF) becomes negative during the stance phases. This implies that the Froude number exceeds 1.0 and the unilateral constraint cannot be guaranteed. The TRW motion therefore gets into running or skipping [12], but such motions cannot be achieved because the mathematical model previously described is assumed to be fixed to the floor. From Fig. 5 (a), we can see that the mechanical energy does not increase monotonically or negative input power emerges. This is because the prismatic joint generates negative force to pull back the point mass. This is also caused by the bilateral constraint which comes from the mathematical model.

The condition of Eq. (26) is for $\theta^+ = 0$ to guarantee overcoming the potential barrier. This condition is, however, sufficient and conservative. We then ease it by introducing the ratio of leg length, $s := l_1/l_0$ [-], and analyze the gait efficiency with respect to s.

In the subsequent numerical simulations, the following statements are considered as judgment conditions for successful walking.

- $s > 1$ is necessary to shift the CoM forward at impact. This also implies that the mechanical energy is restored by extending the stance leg.
- The ground reaction force is always kept positive and unilateral constraint condition always holds.
- $T \geq T_{\rm set}$ holds. (Settling time condition)

Fig. 6 plots the phase portrait of the generated dynamic gait where $s = 1.20$ [-] and $T_{\rm set} = 0.50$ [s]. The TRW started walking from the standing posture with small angular velocity ($\theta(0) = 0$ [rad] and $\dot{\theta}(0) = 0.001$ [rad/s]). The step period and the walking speed converged to 0.5011 [s] and 1.720 [m/s]. Fig. 7 plots the stick diagram of the stance leg and the point mass (hip position) of the TRW, which clearly illustrates the asymmetric impact posture. Fig. 8 shows the time evolutions of the walking motion. Here, (a) is the stance-leg length, (b) the total mechanical energy, (c) the vertical ground reaction force, and (d) the control input. We omitted to plot $l_{\rm d}(t)$ in Fig. 8 (a) because the trajectories of l and $l_{\rm d}(t)$ are identical. From Fig. 8 (c), we can see that the unilateral constraint is maintained during the stance phases. From Fig. 8 (d), we can see that the control input is always kept positive. The mechanical energy is then restored monotonically because of $\dot{l}(t) \equiv \dot{l}_{\rm d}(t) \geq 0$; the sign of the input power becomes nonnegative. This is also supported by Fig. 8 (b).

In this approach, mechanical energy restoration is achieved as a consequence of the stance-leg extension. The primary purpose is not mechanical

energy restoration but creating the asymmetric impact posture. This is the essential difference with our previous methods.

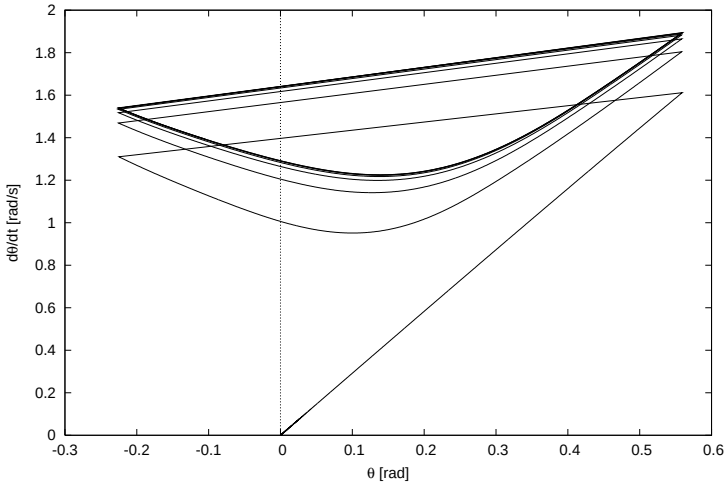

Fig. 6 Phase portrait of stance-leg angle where $T_{\rm set} = 0.50$ [s] and $s = 1.20$ [-]

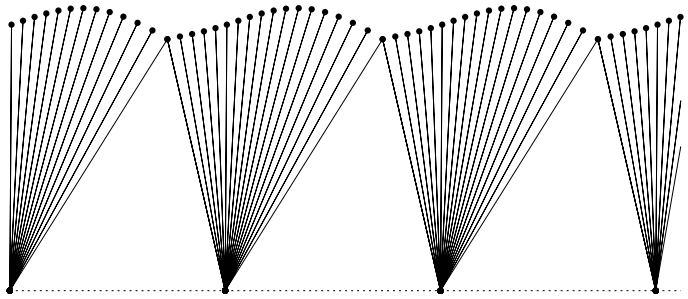

Fig. 7 Stick diagram where $s = 1.20$ and $T_{\rm set} = 0.50$ [s]

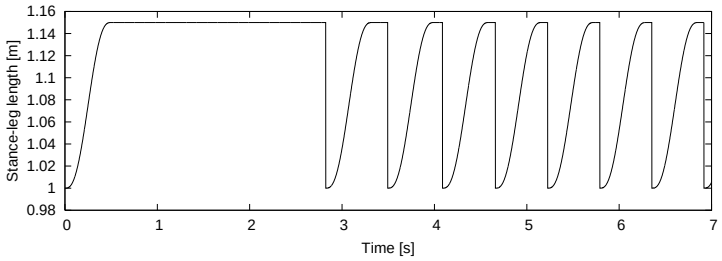

(a) Stance-leg length

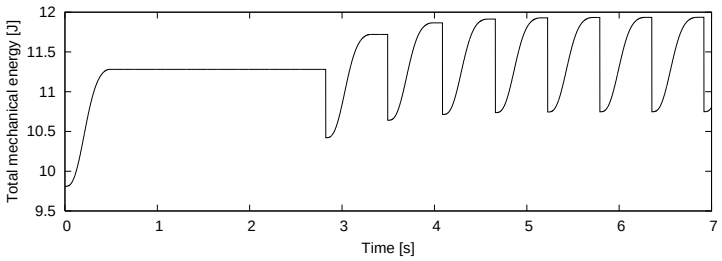

(b) Total mechanical energy

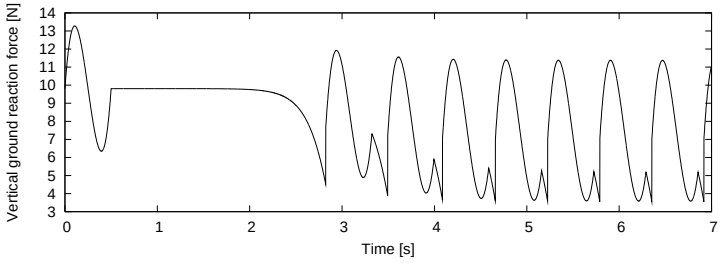

(c) Vertical ground reaction force

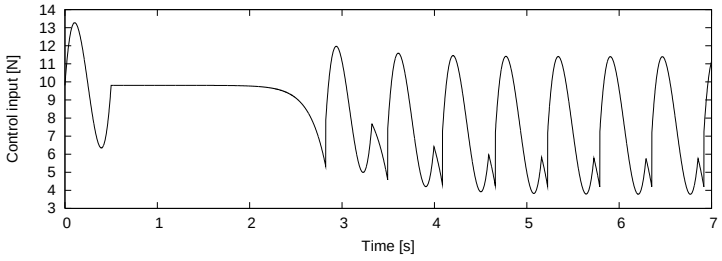

(d) Control input

Fig. 8 Simulation results of dynamic walking based on asymmetric impact posture where $T_{\mathrm{set}} = 0.50$ [s] and $s = 1.20$

2.4 Efficiency analysis

2.4.1 Preliminaries

Let us introduce criterion functions before performing numerical analysis. Let T [s] be the steady step period. For simplicity, every time immediately after impact has been denoted in the following as 0^+ and every time immediately before impact as T^- by resetting the absolute time at every transition instant. Thus T^+ means the same as 0^+. The average walking speed is then defined as

$$v := \frac{1}{T}\int_{0^+}^{T^-} \dot{X}_g \, \mathrm{d}t = \frac{\Delta X_g}{T}, \tag{28}$$

where X_g [m] is the X-position at the CoM and $\Delta X_g := X_g(T^-) - X_g(0^+)$ [m] is equal to the step length shown in Fig. 4. The average input power is also defined as

$$p := \frac{1}{T}\int_{0^+}^{T^-} \left|\dot{l}u\right| \, \mathrm{d}t \tag{29}$$

Energy efficiency is then evaluated by specific resistance (SR):

$$\mathrm{SR} := \frac{p}{Mgv}, \tag{30}$$

which means the expenditure of energy per unit mass and per unit length, and this is a dimension-less quantity [3][4]. The main question of how to attain energy-efficient locomotion rests on how to increase walking speed v while keeping p small.

Let ΔE [J] be the restored mechanical energy per step, then the following magnitude relation holds.

$$p \geq \frac{1}{T}\int_{0^+}^{T^-} \dot{l}u \, \mathrm{d}t = \frac{\Delta E}{T}. \tag{31}$$

The minimum value of SR then becomes

$$\mathrm{SR} \geq \frac{\Delta E}{Mg\Delta X_g}. \tag{32}$$

We have proposed several methods for highly energy-efficient dynamic bipedal walking. For example, $\mathrm{SR} \geq \tan\phi$ [-] in virtual passive dynamic walking (VPDW) where ϕ [rad] is the virtual slope [4], $\mathrm{SR} > 0.01$ [-] in underactuated VPDW with semicircular feet [11], and $\mathrm{SR} > 0.03$ [-] in parametrically-excited dynamic bipedal walking [5]. These values help the evaluation of the following analysis results.

2.4.2 Effects of s and T_{set}

Fig. 9 shows the analysis results of the gait descriptors with respect to s for three values of T_{set}. Here, (a) is the step period, (b) the walking speed, (c) the SR, and (d) the restored mechanical energy. The SR plotted is not the minimum value in Eq. (32) but the actual value.

The maximum s was 1.20 where $T_{\mathrm{set}} = 0.50$ [s]. The feasible region for stable gait generation becomes larger with longer T_{set}. This is because the unilateral constraint cannot be guaranteed when the extending speed is high.

In all cases, the minimum value of s was 1.06. If s becomes smaller than this value, the TRW cannot overcome the potential barrier. As seen from Fig. 9 (a), the step period rapidly lengthens as s approaches 1.06. This is because the CoM is strongly stalled around the potential barrier.

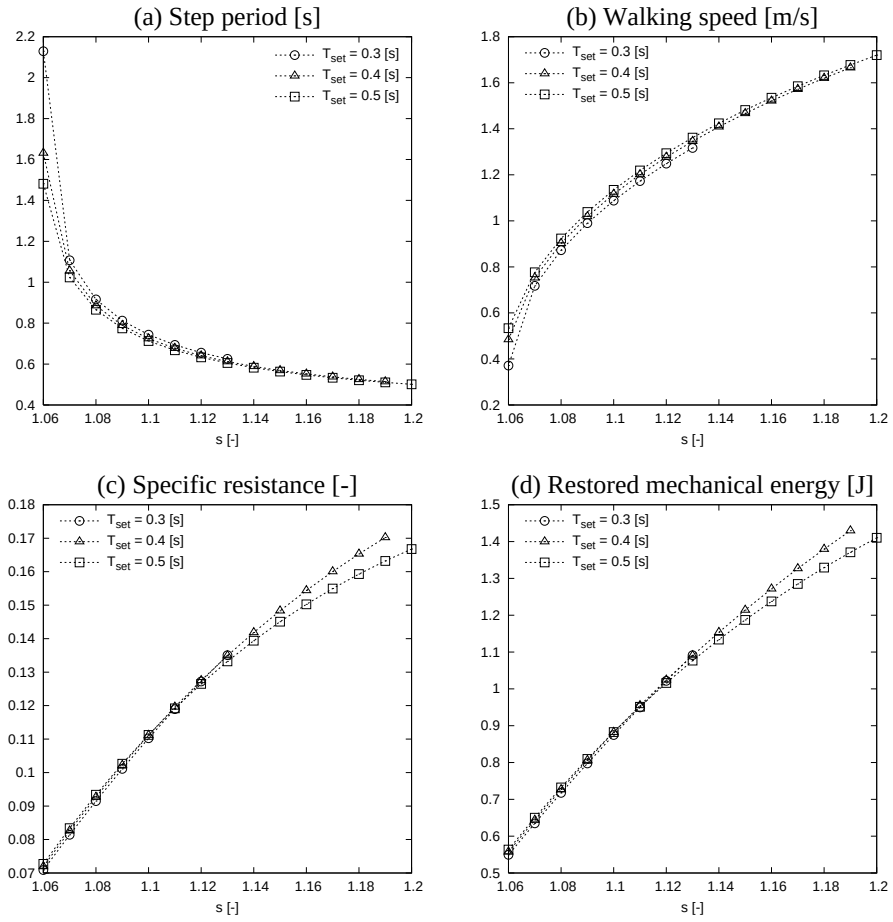

Fig. 9 Gait descriptors with respect to s for three values of T_{set}

From Figs. 9 (b) and (d), we can see that the walking speed and the restored mechanical energy monotonically increase as s increases for all $T_{\rm set}$. These imply that the forward motion is accelerated monotonically with respect to the extended leg length. From Fig. 9 (c), however, we can see that the energy efficiency grows worse in return for it. ΔE monotonically increases with the increase of s without generating the negative input power, whereas the step length in Fig. 4 satisfies $\Delta X_g^2 = l_0^2 + l_1^2 - 2l_0 l_1 \cos\alpha$ and its derivative with respect to l_1 becomes

$$\frac{\partial \Delta X_g^2}{\partial l_1} = 2l_0(s - \cos\alpha) > 0 \tag{33}$$

because of $s > 1$. Therefore, ΔX_g also monotonically increases with the increase of s. We then conclude that the increasing rate of ΔE is much larger than that of ΔX_g.

3 Extension to Planar Telescopic-legged Biped Robot

This section extends our method to a planar telescopic-legged biped robot and discusses the role of asymmetric shape of human foot from the ankle-brake effect point of view.

3.1 Modeling of telescopic-legged biped robot

3.1.1 Dynamic equation

Fig. 10 shows the planar telescopic-legged biped model. Let the stance leg and swing leg be Leg 1 and Leg 2, and $\boldsymbol{q}_j = \begin{bmatrix} x_j & z_j & \theta_j & b_j \end{bmatrix}^{\rm T}$ be the generalized coordinate vector for Leg j. The corresponding dynamic equation for Leg j becomes

$$\boldsymbol{M}_j(\boldsymbol{q}_j)\ddot{\boldsymbol{q}}_j + \boldsymbol{h}_j(\boldsymbol{q}_j, \dot{\boldsymbol{q}}_j) = \boldsymbol{0}_{4\times 1}, \tag{34}$$

where

$$\boldsymbol{M}_j(\boldsymbol{q}_j) = \begin{bmatrix} m + \frac{m_H}{2} & 0 & \left(ma + \frac{m_H}{2}(a + b_j)\right)\cos\theta_j & \frac{m_H}{2}\sin\theta_j \\ & m + \frac{m_H}{2} & -\left(ma + \frac{m_H}{2}(a + b_j)\right)\sin\theta_j & \frac{m_H}{2}\cos\theta_j \\ & & ma^2 + \frac{m_H}{2}(a + b_j)^2 & 0 \\ \text{Sym.} & & & \frac{m_H}{2} \end{bmatrix},$$

$$\boldsymbol{h}_j(\boldsymbol{q}_j, \dot{\boldsymbol{q}}_j) = \begin{bmatrix} \dot\theta_j\left(m_H\dot b_j\cos\theta_j - \left(ma + \frac{m_H}{2}(a + b_j)\right)\dot\theta_j\sin\theta_j\right) \\ -\dot\theta_j\left(m_H\dot b_j\sin\theta_j + \left(ma + \frac{m_H}{2}(a + b_j)\right)\dot\theta_j\cos\theta_j\right) \\ m_H\dot\theta_j\dot b_j(a + b_j) \\ -\frac{m_H}{2}\dot\theta_j^2(a + b_j) \end{bmatrix}$$

$$+ \begin{bmatrix} 0 \\ \left(m + \frac{m_H}{2}\right)g \\ -\left(ma + \frac{m_H}{2}(a + b_j)\right)g\sin\theta_j \\ \frac{m_H}{2}g\cos\theta_j \end{bmatrix}.$$

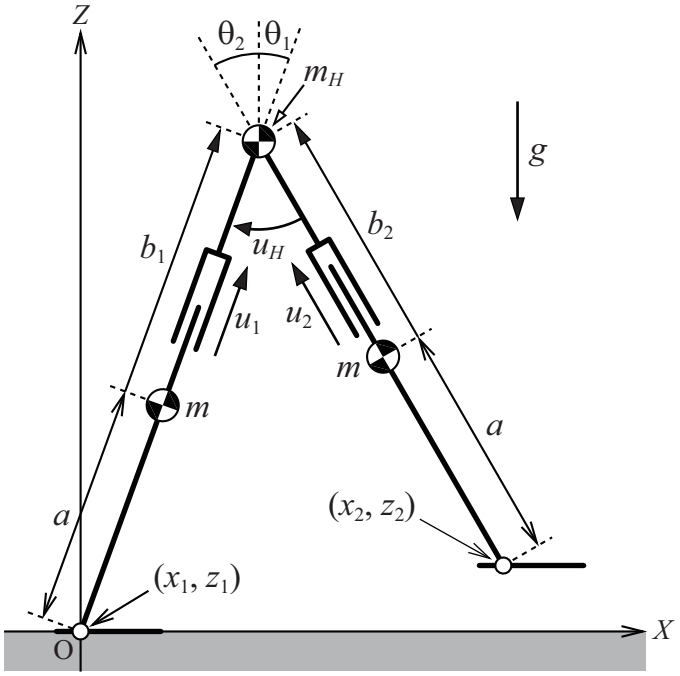

Fig. 10 Model of planar telescopic-legged biped robot with flat feet

We then augment them by adding the holonomic constraint forces and control inputs. We assume that the two legs are connected at the hip joint without incorporating joint friction. For simplifying the gait analysis, we also assume that the foot mass and thin are ignorable and the dynamics of feet does not affect the walking motion at all. Point contact of the stance leg with the ground is then always maintained. Let $\boldsymbol{q} = \left[\boldsymbol{q}_1^{\mathrm{T}}\ \boldsymbol{q}_2^{\mathrm{T}}\right]^{\mathrm{T}}$ be the generalized coordinate vector of the augmented system, the dynamic equation then becomes

$$\boldsymbol{M}(\boldsymbol{q})\ddot{\boldsymbol{q}} + \boldsymbol{h}(\boldsymbol{q}, \dot{\boldsymbol{q}}) = \boldsymbol{S}\boldsymbol{u} + \boldsymbol{J}(\boldsymbol{q})^{\mathrm{T}}\boldsymbol{\lambda}, \quad \boldsymbol{J}(\boldsymbol{q})\dot{\boldsymbol{q}} = \boldsymbol{0}_{4\times 1}, \tag{35}$$

where $\boldsymbol{S}\boldsymbol{u} \in \mathbb{R}^8$ is the control input vector, $\boldsymbol{J}(\boldsymbol{q})^{\mathrm{T}}\boldsymbol{\lambda} \in \mathbb{R}^8$ is the holonomic constraint force vector for connecting the two legs. The terms in Eq. (35) are detailed as

$$\boldsymbol{M}(\boldsymbol{q}) = \begin{bmatrix} \boldsymbol{M}_1(\boldsymbol{q}_1) & \boldsymbol{0}_{4\times 4} \\ \boldsymbol{0}_{4\times 4} & \boldsymbol{M}_2(\boldsymbol{q}_2) \end{bmatrix}, \quad \boldsymbol{h}(\boldsymbol{q}, \dot{\boldsymbol{q}}) = \begin{bmatrix} \boldsymbol{h}_1(\boldsymbol{q}_1, \dot{\boldsymbol{q}}_1) \\ \boldsymbol{h}_2(\boldsymbol{q}_2, \dot{\boldsymbol{q}}_2) \end{bmatrix}.$$

By eliminating $\boldsymbol{\lambda}$ from Eq. (35), the dynamic equation is arranged as

$$\boldsymbol{M}(\boldsymbol{q})\ddot{\boldsymbol{q}} = \boldsymbol{Y}(\boldsymbol{q})\left(\boldsymbol{S}\boldsymbol{u} - \boldsymbol{h}(\boldsymbol{q}, \dot{\boldsymbol{q}})\right) - \boldsymbol{J}(\boldsymbol{q})^{\mathrm{T}}\boldsymbol{X}(\boldsymbol{q})^{-1}\dot{\boldsymbol{J}}(\boldsymbol{q}, \dot{\boldsymbol{q}})\dot{\boldsymbol{q}}, \tag{36}$$

$$\boldsymbol{Y}(\boldsymbol{q}) := \boldsymbol{I}_8 - \boldsymbol{J}(\boldsymbol{q})^{\mathrm{T}}\boldsymbol{X}(\boldsymbol{q})^{-1}\boldsymbol{J}(\boldsymbol{q})\boldsymbol{M}(\boldsymbol{q})^{-1}, \tag{37}$$

$$\boldsymbol{X}(\boldsymbol{q}) := \boldsymbol{J}(\boldsymbol{q})\boldsymbol{M}(\boldsymbol{q})^{-1}\boldsymbol{J}(\boldsymbol{q})^{\mathrm{T}}. \tag{38}$$

The control input vector is also detailed as

$$\boldsymbol{S}\boldsymbol{u} = \begin{bmatrix} 0 & 0 & 0 \\ 0 & 0 & 0 \\ 0 & 0 & 1 \\ 1 & 0 & 0 \\ 0 & 0 & 0 \\ 0 & 0 & 0 \\ 0 & 0 & -1 \\ 0 & 1 & 0 \end{bmatrix} \begin{bmatrix} u_1 \\ u_2 \\ u_H \end{bmatrix}. \tag{39}$$

The ankle-joint torque, u_A, is added later.

3.1.2 Transition equations

The positions are exchanged in accordance with the geometrical conditions as follows:

$$\begin{aligned} &x_1^+ = 0, \quad z_1^+ = 0, \quad \theta_1^+ = \theta_2^-, \quad \theta_2^+ = \theta_1^-, \\ &x_2^+ = x_1^+ + l_1 \sin\theta_1^+ - l_2 \sin\theta_2^+ = -x_2^-, \\ &z_2^+ = z_1^+ + l_1 \cos\theta_1^+ - l_2 \cos\theta_2^+ = -z_2^- = 0. \end{aligned}$$

Where $l_j := a + b_j$ is the length of Leg j.

Next, the transition equations for the velocities are described. We first calculate the velocities immediately after impact without switching the legs. After that, we exchange the velocities of Leg 1 for those of Leg 2. Assuming that Leg 1 leaves the floor immediately after impact, the inelastic collision is modeled as

$$\boldsymbol{M}(\boldsymbol{q})\dot{\boldsymbol{q}}^+ = \boldsymbol{M}(\boldsymbol{q})\dot{\boldsymbol{q}}^- - \boldsymbol{J}_I(\boldsymbol{q})^{\mathrm{T}}\boldsymbol{\lambda}_I, \tag{40}$$

$$\boldsymbol{J}_I(\boldsymbol{q})\dot{\boldsymbol{q}}^+ = \boldsymbol{0}_{7\times 1}. \tag{41}$$

The Jacobian matrix $\boldsymbol{J}_I(\boldsymbol{q}) \in \mathbb{R}^{7\times 8}$ is derived as follows. Also in this case, we assume that there is a high friction at the contact point of the legs' ends with the ground. The conditions that the end-point of Leg 2 does not slide immediately after impact are given by

$$\dot{x}_2^+ = 0, \quad \dot{z}_2^+ = 0. \tag{42}$$

We also assume that the prismatic joints of the legs are mechanically locked at impact, and the conditions are given by

$$\dot{b}_1^+ = 0, \quad \dot{b}_2^+ = 0. \tag{43}$$

In addition, the conditions that the hip positions of both legs are identical are given by

$$\frac{\mathrm{d}}{\mathrm{d}t}\left(x_1 + l_1 \sin\theta_1\right)^+ = \frac{\mathrm{d}}{\mathrm{d}t}\left(x_2 + l_2 \sin\theta_2\right)^+, \tag{44}$$

$$\frac{\mathrm{d}}{\mathrm{d}t}\left(z_1 + l_1 \cos\theta_1\right)^+ = \frac{\mathrm{d}}{\mathrm{d}t}\left(z_2 + l_2 \cos\theta_2\right)^+, \tag{45}$$

and these lead to

$$\dot{x}_1^+ + l_1\dot{\theta}_1^+ \cos\theta_1 + \dot{b}_1^+ \sin\theta_1 = \dot{x}_2^+ + l_2\dot{\theta}_2^+ \cos\theta_2 + \dot{b}_2^+ \sin\theta_2, \tag{46}$$

$$\dot{z}_1^+ - l_1\dot{\theta}_1^+ \sin\theta_1 + \dot{b}_1^+ \cos\theta_1 = \dot{z}_2^+ - l_2\dot{\theta}_2^+ \sin\theta_2 + \dot{b}_2^+ \cos\theta_2. \tag{47}$$

To cancel out the tracking error, we further consider another condition that the relative hip-joint, $\theta_H := \theta_1 - \theta_2$ is mechanically locked at impact:

$$\dot{\theta}_H^+ = 0. \tag{48}$$

Following the above conditions, we can precisely achieve $\boldsymbol{y} \equiv \boldsymbol{y}_{\mathrm{d}}(t)$ without PD feedback because all velocities of the output immediately after impact, $\dot{\boldsymbol{y}}^+$, become zero. The control input can be specified only by feed-forward of the desired acceleration, and we can examine the gait efficiency reflecting the desired trajectories accurately.

Summarizing the above seven velocity constraint conditions of (42), (43), (46), (47) and (48), matrix $\boldsymbol{J}_I(\boldsymbol{q}) \in \mathbb{R}^{7\times 8}$ is specified as follows:

$$\boldsymbol{J}_I(\boldsymbol{q}) = \begin{bmatrix} 1 & 0 & J_{13} & J_{14} & -1 & 0 & J_{17} & J_{18} \\ 0 & 1 & J_{23} & J_{24} & 0 & -1 & J_{27} & J_{28} \\ 0 & 0 & 0 & 0 & 1 & 0 & 0 & 0 \\ 0 & 0 & 0 & 0 & 0 & 1 & 0 & 0 \\ 0 & 0 & 0 & 1 & 0 & 0 & 0 & 0 \\ 0 & 0 & 0 & 0 & 0 & 0 & 0 & 1 \\ 0 & 0 & 1 & 0 & 0 & 0 & -1 & 0 \end{bmatrix}, \tag{49}$$

where

$$J_{13} = l_1\cos\theta_1, \quad J_{14} = \sin\theta_1, \quad J_{17} = -l_2\cos\theta_2, \quad J_{18} = -\sin\theta_2,$$
$$J_{23} = -l_1\sin\theta_1, \quad J_{24} = \cos\theta_1, \quad J_{27} = l_2\sin\theta_2, \quad J_{28} = -\cos\theta_2.$$

We can finally accomplish the transition by replacing $\dot{\boldsymbol{q}}_1^+$ with $\dot{\boldsymbol{q}}_2^+$ in $\dot{\boldsymbol{q}}^+ = \begin{bmatrix} \dot{\boldsymbol{q}}_1^+ & \dot{\boldsymbol{q}}_2^+ \end{bmatrix}^{\mathrm{T}}$.

Matrix $\boldsymbol{J}(\boldsymbol{q})$ in Eq. (35) is also derived as

$$\boldsymbol{J}(\boldsymbol{q}) = \begin{bmatrix} 1 & 0 & J_{13} & J_{14} & -1 & 0 & J_{17} & J_{18} \\ 0 & 1 & J_{23} & J_{24} & 0 & -1 & J_{27} & J_{28} \\ 1 & 0 & 0 & 0 & 0 & 0 & 0 & 0 \\ 0 & 1 & 0 & 0 & 0 & 0 & 0 & 0 \end{bmatrix} =: \begin{bmatrix} \boldsymbol{J}_1(\boldsymbol{q}) \\ \boldsymbol{J}_2(\boldsymbol{q}) \\ \boldsymbol{J}_3 \\ \boldsymbol{J}_4 \end{bmatrix}. \tag{50}$$

The holonomic constraint force vector in Eq. (35) can be divided into

$$\boldsymbol{J}(\boldsymbol{q})^{\mathrm{T}}\boldsymbol{\lambda} = \boldsymbol{J}_1(\boldsymbol{q})^{\mathrm{T}}\lambda_1 + \boldsymbol{J}_2(\boldsymbol{q})^{\mathrm{T}}\lambda_2 + \boldsymbol{J}_3^{\mathrm{T}}\lambda_3 + \boldsymbol{J}_4^{\mathrm{T}}\lambda_4, \tag{51}$$

and each undetermined multiplier λ_i corresponds to the forces in Fig. 11. λ_4 is identical to the vertical ground reaction force, and X-position of the ZMP is then calculated by

$$X_{\mathrm{zmp}} = -\frac{u_A}{\lambda_4}. \tag{52}$$

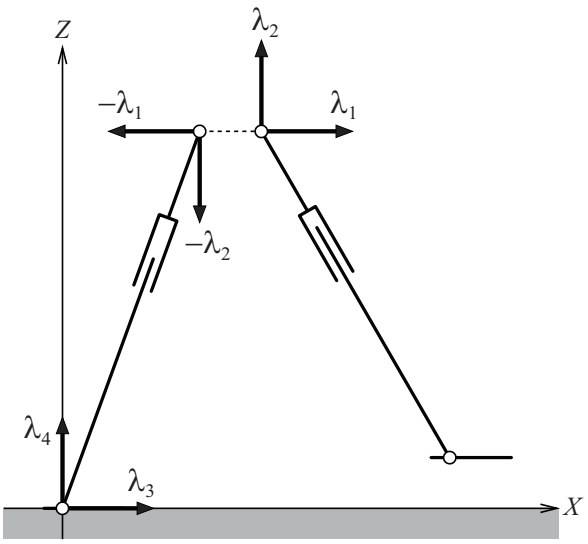

Fig. 11 Four holonomic constraint forces

3.2 Output following control

We choose the two telescopic-leg lengths and the relative hip angle as the control output. The output vector, $\boldsymbol{y} \in \mathbb{R}^3$, is then defined as

$$\boldsymbol{y} = \begin{bmatrix} b_1 \\ b_2 \\ \theta_H \end{bmatrix} = \boldsymbol{S}^{\mathrm{T}} \boldsymbol{q}, \tag{53}$$

and its second-order derivative with respect to time becomes

$$\ddot{\boldsymbol{y}} = \boldsymbol{S}^{\mathrm{T}} \ddot{\boldsymbol{q}} = \boldsymbol{A}(\boldsymbol{q})\boldsymbol{u} - \boldsymbol{B}(\boldsymbol{q}, \dot{\boldsymbol{q}}), \tag{54}$$

where

$$\boldsymbol{A}(\boldsymbol{q}) := \boldsymbol{S}^{\mathrm{T}} \boldsymbol{M}(\boldsymbol{q})^{-1} \boldsymbol{Y}(\boldsymbol{q}) \boldsymbol{S}, \tag{55}$$

$$\boldsymbol{B}(\boldsymbol{q}, \dot{\boldsymbol{q}}) := \boldsymbol{S}^{\mathrm{T}} \boldsymbol{M}(\boldsymbol{q})^{-1} \left(\boldsymbol{Y}(\boldsymbol{q}) \boldsymbol{h}(\boldsymbol{q}, \dot{\boldsymbol{q}}) + \boldsymbol{J}(\boldsymbol{q})^{\mathrm{T}} \boldsymbol{X}(\boldsymbol{q})^{-1} \dot{\boldsymbol{J}}(\boldsymbol{q}, \dot{\boldsymbol{q}}) \dot{\boldsymbol{q}} \right). \tag{56}$$

Then we can consider the following control input for achieving $\boldsymbol{y} \to \boldsymbol{y}_{\mathrm{d}}$.

$$\boldsymbol{u} = \boldsymbol{A}(\boldsymbol{q})^{-1} \left(\boldsymbol{v} + \boldsymbol{B}(\boldsymbol{q}, \dot{\boldsymbol{q}}) \right) \tag{57}$$

$$\boldsymbol{v} = \ddot{\boldsymbol{y}}_{\mathrm{d}} + \boldsymbol{K}_{\mathrm{D}} \left(\dot{\boldsymbol{y}}_{\mathrm{d}} - \dot{\boldsymbol{y}} \right) + \boldsymbol{K}_{\mathrm{P}} \left(\boldsymbol{y}_{\mathrm{d}} - \boldsymbol{y} \right) \tag{58}$$

By adding the condition of Eq. (48), all elements of $\dot{\boldsymbol{y}}^+$ become zero and the trajectory tracking control without any tracking errors, $\boldsymbol{y} \equiv \boldsymbol{y}_{\mathrm{d}}(t)$, is achieved only by the feed-forward control of the desired accelerations.

The time-dependent desired trajectories are specified as 5-order functions for smoothly interpolating between the boundary conditions, and all the outputs are smoothly controlled from the initial conditions to the final ones in each step.

3.3 Efficiency analysis

3.3.1 Starting from standing posture

We first consider a starting control and stable gait generation from a static standing posture. The robot starts walking from a standing posture ($b_1 = b_2 = b$, $\theta_1 = \theta_2 = 0$) and static condition ($\dot{\theta}_1 = \dot{\theta}_2 = 0$, $\dot{b}_1 = \dot{b}_2 = 0$), and generate the dynamic gait while updating the desired trajectories in accordance with the following strategy.

The telescopic-leg length of the stance leg, b_1, is controlled to follow its desired time-dependent trajectory, $b_{1\mathrm{d}}(t)$, from the length immediately after impact, b_1^+, to the terminal value, $b + \Delta b$. We consider a time-dependent 5-order function to smoothly interpolate the values, and update the coefficients at every impact. The telescopic-leg length of the swing leg, b_2, and the relative hip angle, θ_H, are also controlled to follow their desired trajectories, $b_{2\mathrm{d}}(t)$ and $\theta_{H\mathrm{d}}(t)$, in the same manner as b_1. This will result in that, after the first impact, b_1 is controlled from $b - \Delta b$ to $b + \Delta b$, b_2 is controlled from $b + \Delta b$ to $b - \Delta b$, and θ_H is controlled from $-\alpha$ to α by following their smooth desired trajectories. The telescopic-legged rimless wheel must start with a small initial velocity to fall down, whereas a biped robot can start the walking from a static standing posture only by creating the first impact posture because this results in shifting the CoM forward.

Fig. 12 shows the simulation results of dynamic walking from a static standing posture where $\Delta b = 0.05$ [m]. We can see that a stable 1-period gait is generated. Fig. 13 shows the stick diagram for one cycle. The system parameters were chosen as listed in Table 1. The desired settling time for shortening the swing-leg length, $T_{\mathrm{set}}^{(2)}$, were chosen as a shorter value than others to guarantee the foot clearance.

The most remarkable result is the high walking speed. In this case, the walking speed converged to 1.31 [m/s]. It is reported that the average walking speed of adult humans is 82 [m/min] (= 1.367 [m/s]) in [13]. We can find that the walking speed of the generated gait approaches to that of humans. Compared to the results of VPDW [4] and energy tracking control [2], the obtained walking speed is found to be remarkably fast. Although we cannot avoid the deterioration of energy-efficiency, the proposed approach enables the robot to generate a remarkably high-speed gait that the previous methods

Table 1 Physical and control parameters of biped walking system

m_H	10.0	kg	α	0.60	rad
m	5.0	kg	$T_{\mathrm{set}}^{(1)}$	0.40	s
a	0.50	m	$T_{\mathrm{set}}^{(2)}$	0.30	s
b	0.50	m	$T_{\mathrm{set}}^{(H)}$	0.40	s

could not achieve. Note also that the gait generation does not depend on the effect of semicircular feet [11].

From Fig. 12(d), we can see that sufficiently large vertical GRF is generated during stance phases compared to the case of the TRW. This is because the lower part of the leg is heavy.

From Fig. 12(e), we can see that negative input power occurs during posterior half of cycle. This is caused by the tracking control to the time-dependent desired trajectories. As mentioned later, the gait generation becomes impossible as Δb further decreases. In this case, the robot must utilize the ankle-joint actuation, or it cannot obtain sufficient driving force to overcome the potential barrier.

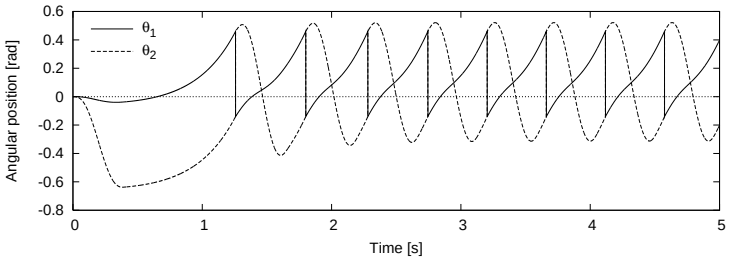

(a) Angular position

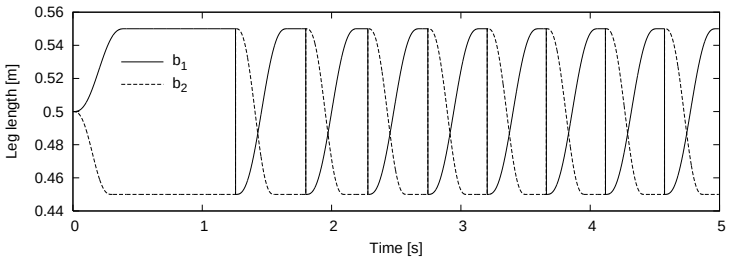

(b) Telescopic-leg length

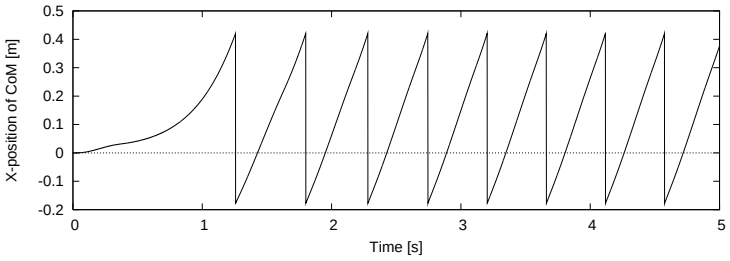

(c) X-position of CoM

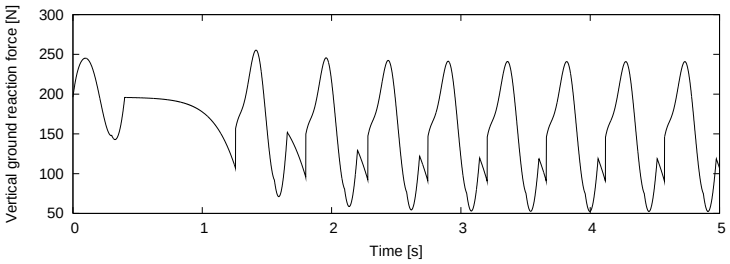

(d) Vertical ground reaction force

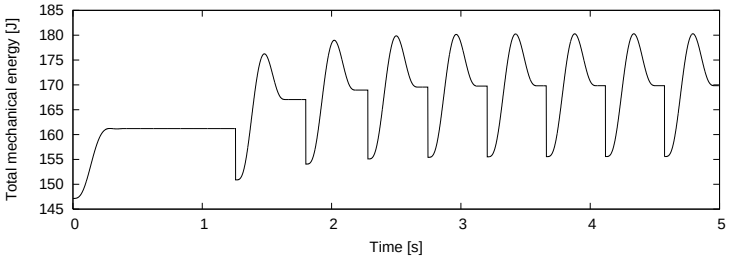

(e) Total mechanical energy

Fig. 12 Simulation results of dynamic walking from standing posture where $\Delta b = 0.05$ [m]

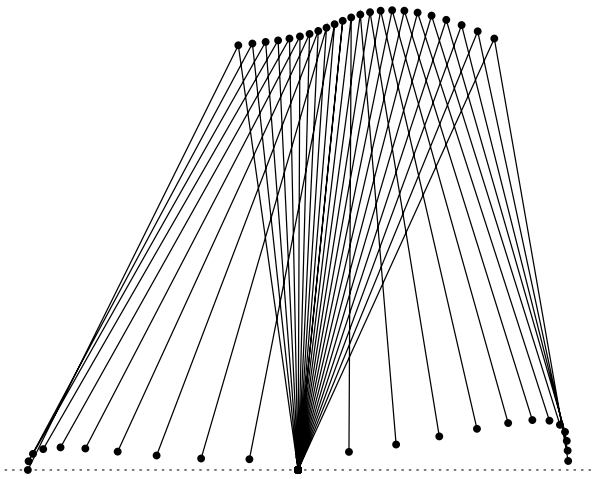

Fig. 13 Stick diagram for steady gait where $\Delta b = 0.05$ [m]

3.3.2 Efficiency analysis considering ankle-joint torque

In the case of the TRW, remarkably high-speed level gaits near-running were generated. In return for it, however, the motion was too rapid to satisfy the desired settling-time condition for the telescopic-leg actuation. As a candidate of the solution to this problem, a brake effect by the ankle-joint actuation can be considered. By driving the stance leg backward, we can extend the time margin, i.e., the step period.

In this section, we consider the foot mechanism with an elastic element as shown in Fig. 14, and apply its effect as the ankle-joint torque to the robot. We assume that the elastic element becomes natural length when $\theta_1 = 0$, and the ankle-joint torque, u_A, is then given by

$$u_A = -k\theta_1, \tag{59}$$

where k [N·m] is a positive constant which stands for the elastic coefficient. $X_{\rm zmp}$ calculated by Eq. (52) accordingly becomes $k\theta_1/\lambda_4$ [m]. The ankle-joint torque vector also becomes

$$\boldsymbol{S}_A u_A = \begin{bmatrix} 0 & 0 & 1 & 0 & 0 & 0 & 0 & 0 \end{bmatrix}^{\rm T} u_A, \tag{60}$$

and we add this to the right-hand side of Eq. (35) to calculate $\boldsymbol{\lambda}$. Also note that $\boldsymbol{h}(\boldsymbol{q}, \dot{\boldsymbol{q}})$ in Eq. (56) must be replaced with $\boldsymbol{h}(\boldsymbol{q}, \dot{\boldsymbol{q}}) - \boldsymbol{S}_A u_A$ to calculate $\boldsymbol{B}(\boldsymbol{q}, \dot{\boldsymbol{q}})$.

Fig. 15 shows the gait descriptors with respect to Δb changing it by 0.005 [m]. We plotted the results, however, only in the case the generated gait was 1-period stable. The elastic coefficient, k, was chosen as 0.0, 5.0, 10.0, 15.0 and 20.0 [N·m].

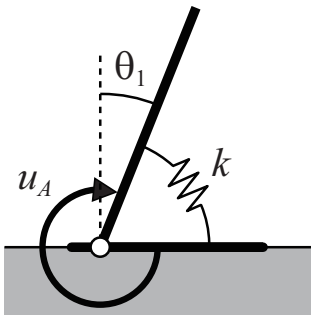

Fig. 14 Foot mechanism with elastic element

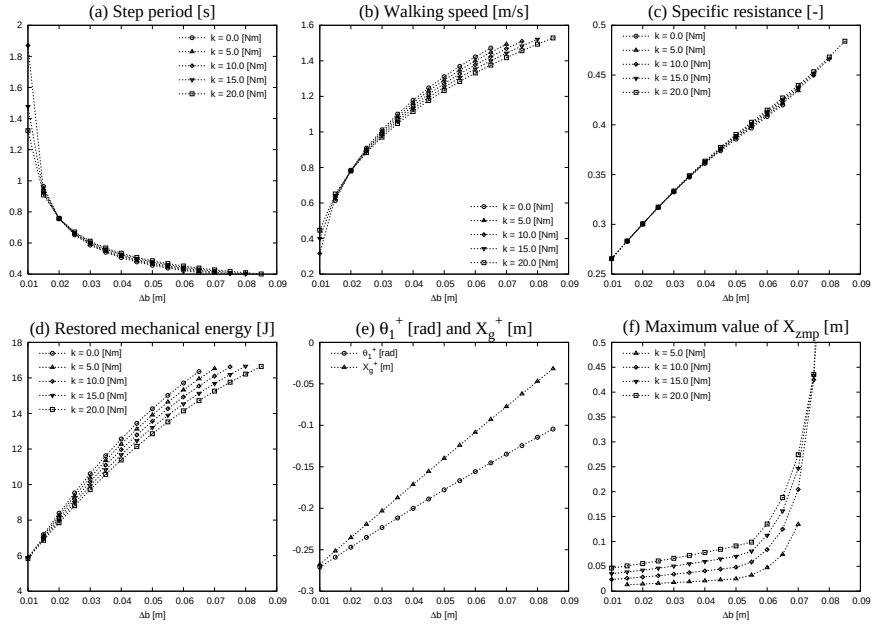

Fig. 15 Gait descriptors with respect to Δb for five values of k

From Fig. 15(a), we can see that the step period monotonically decreases with the increase of Δb in all cases. In addition, enough settling-time margin is created when k is large. The maximum desired settling time is chosen as $T_{\rm set}^{(1)} = T_{\rm set}^{(H)} = 0.40$ [s], and the step period must be longer than it. In all cases, this condition becomes impossible to be met as the impact posture is more asymmetrized. When Δb is large, the larger k becomes, the longer the settling-time margin becomes by the brake effect of u_A. When Δb is small ($\Delta b \leq 0.02$ [m]), however, this tendency reverses. In addition, stable gaits are generated even if $\Delta b = 0.01$ [m] where $k = 10.0$, 15.0, and 20.0. This is because u_A becomes positive during the first phase of cycle or when θ_1 is negative, and it helps to overcome the potential barrier.

From Fig. 15(b), we can see that the walking speed monotonically increases with the increase of Δb in all cases. The step length is identical to the horizontal distance the CoM travels, ΔX_g [m], and it satisfies

$$\begin{aligned}\Delta X_g^2 &= (a+b+\Delta b)^2 + (a+b-\Delta b)^2 \\ &\quad -2(a+b+\Delta b)(a+b-\Delta b)\cos\alpha, \end{aligned} \tag{61}$$

$$\frac{\partial \Delta X_g^2}{\partial \Delta b} = 4\left(1+\cos\alpha\right)\Delta b. \tag{62}$$

Then we can find that it monotonically increases with respect to Δb. Since the walking speed is calculated by Eq. (28), we can conclude that the walking speed increases by the synergistic effect of the increment of ΔX_g and the decrement of step period. The increasing tendency of ΔX_g is less than that of Δb, however, the walking speed fundamentally changes inversely proportional to the step period.

From Fig. 15(c), we can see that the SR monotonically increases with the increase of Δb in all cases. It is natural that the consumed energy increases with respect to the leg extension and its control speed, and this result implies that the increasing tendency of the consumed energy (average input power) is more than that of the walking speed. As a candidate of solution to improve the energy-efficiency, extending the desired settling-time in accordance with the step period extended by the brake effect of u_A can be considered. We would like to leave the detailed analysis for another opportunity.

Note that we did not take u_A into account to calculate the SR because it is not an input torque but an elastic force. The average input power is thus defined as

$$p = \frac{1}{T}\int_{0^+}^{T^-} \left(\left|\dot{b}_1 u_1\right| + \left|\dot{b}_2 u_2\right| + \left|\dot{\theta}_H u_H\right|\right) \mathrm{d}t. \tag{63}$$

Fig. 15(e) plots θ_1 and X_g immediately after impact. We plotted the analysis results where $k = 20.0$ only because the impact posture is uniquely determined according to Δb regardless of k. In all cases, the values of X_g^+ are negative, that is, the generated impact postures cannot guarantee to overcome the potential barrier. Also the values of θ_1^+ are always negative. This implies that the hip position does not shift anterior to the forefoot point at impact. Let's consider these results from the angular momentum point of view. Let L [kg·m^2/s] be the angular momentum around the stance-foot point, its time-derivative satisfies

$$\dot{L} = u_A + MgX_g, \tag{64}$$

where M [kg] is the robot's total mass. The angular momentum draws a curve convex downward with respect to time in the presence of potential barrier. If the robot achieves the sufficient condition for overcoming the potential barrier, $X_g^+ \geq 0$, however, $\dot{L}$ becomes always positive and L then monotonically increases. The analysis results imply that a dynamic gait achieving $X_g^+ \geq 0$ or $\dot{L} \geq 0$ is extremely high-speed and is hard to be realized. In other words, achieving $X_g^+ < 0$ or creating the phase with $\dot{L} < 0$ prevents the excessive forward acceleration for achieving a stable walking.

Fig. 15(f) plots the maximum values of $X_{\rm zmp}$ calculated by Eq. (52). We omitted the result where $k = 0.0$ [N·m] because the value is always kept zero. We can see that the values monotonically increase with respect to Δb and there is a significant change in the increasing tendency of the maximum ZMP around $\Delta b = 0.055$ [m] in all cases. Fig. 16 shows the steady ZMP pattern with respect to time for two values of Δb where $k = 20.0$. In the case of $\Delta b = 0.040$ [m], there is a change or indifferentiable point in the ZMP motion immediately prior to impact. This is because the telescopic-leg actuation is completed at this instant (the desired settling time, $t = T_{\rm set}^{(1)}$), and the robot begins to fall down as a 1-dof rigid body. As a result, the peak immediately prior to the settling time yields the maximum value of ZMP. Whereas in the case of $\Delta b = 0.070$ [m], there is little time-margin and the heel-strike occurs immediately after the settling time, and the peak during the control phases yields the maximum ZMP. There are two common features in both cases; one is that the ZMP moves from heel to toe, and another is that the ZMP remains within the area anterior to the ankle joint during most part of cycle. These are similar to human walking.

Note that the forefoot must be longer than 30 [cm] where $k = 20.0$ [N·m] and $\Delta b > 0.07$ [m] as shown in Fig. 15 (f). In humans, as shown in Fig. 17, the heel would rise up or the motion of forefoot weight-bearing [13] would start in this case. Also in robot walking, this situation would occur because the robot's foot length is limited. The ZMP-based approach can be regarded as the method for treating a legged robot as a robotic arm fixed on the floor. Foot flat weight-bearing is a condition that must be maintained for performing ZMP-based control. The simulation results in this section imply, however, that forefoot weight-bearing is a natural motion as a sequence of achieving efficient dynamic walking. In the future, we should analyze dynamic walking

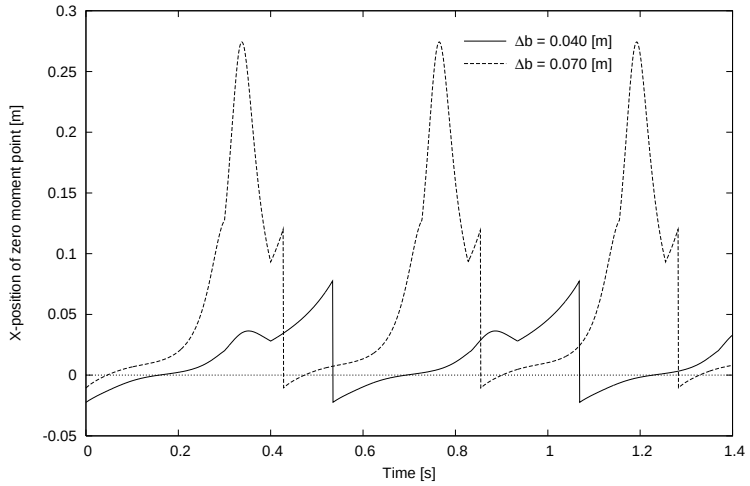

Fig. 16 Time evolutions of $X_{\rm zmp}$ for two values of Δb

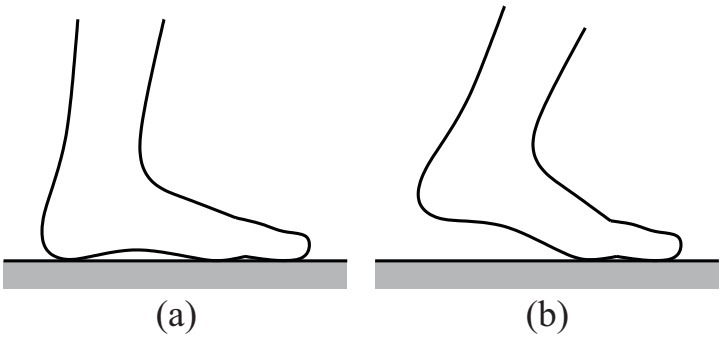

Fig. 17 Foot flat weight-bearing (a) and forefoot weight-bearing (b)

incorporating foot action for systematizing the methods for achieving more natural and efficient legged locomotion.

4 Conclusion and Future Work

In this paper, we have proposed a novel gait generation method based on forward-tilting impact posture for planar limit cycle walkers with telescopic legs, and have confirmed the validity of the method through numerical investigations. The simulation results showed that remarkably high-speed level dynamic gaits can be generated only by tilting the impact posture slightly forward. We also discussed the role of asymmetric shape of human foot from the viewpoint of the ankle brake effect. The simulation results showed that the ankle-joint torque as a brake is effective to generate a stable gait in terms of extending the time margin, and that the toe-side must be longer than the heel-side for covering the ZMP motion.

The greatest contribution of our study is to provide a novel insight that bipedal movement is generated not by forward propulsion but by braking of falling forward. We believe that this understanding would help to achieve efficient, high-speed, and human-like dynamic bipedal walking.

As shown in Fig. 18, we can consider other approaches to creating forward tilting impact posture; utilizing knee-bending, forefeet rigidly attached to the legs, and upper body (counterweight). Now we are examining these effects and the results will be reported in our future paper.

References

1. T. McGeer, "Passive dynamic walking," *Int. J. of Robotics Research*, Vol. 9, No. 2, pp. 62–82, April 1990.
2. A. Goswami, B. Espiau and A. Keramane, "Limit cycles in a passive compass gait biped and passivity-mimicking control laws," *Autonomous Robots*, Vol. 4, No. 3, pp. 273–286, Sept. 1997.

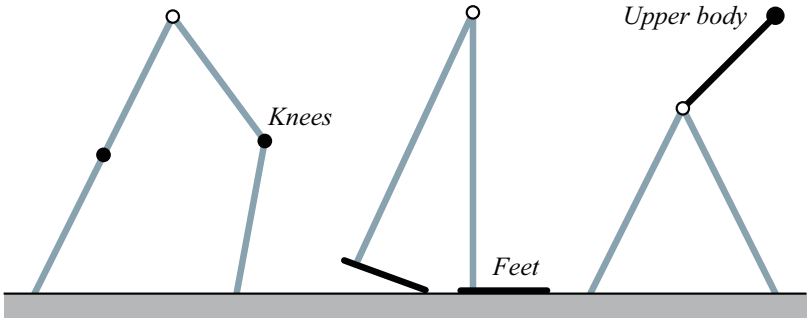

Fig. 18 Several approaches to forward-tilting impact posture

3. S. Collins, A. Ruina, R. Tedrake and M. Wisse, "Efficient bipedal robots based on passive-dynamic walkers," *Science*, Vol. 307, No. 5712, pp. 1082–1085, Feb. 2005.
4. F. Asano, Z.-W. Luo and M. Yamakita, "Biped gait generation and control based on a unified property of passive dynamic walking," *IEEE Trans. on Robotics*, Vol. 21, No. 4, pp. 754–762, Aug. 2005.
5. F. Asano and Z.-W. Luo, "Energy-efficient and high-speed dynamic biped locomotion based on principle of parametric excitation," *IEEE Trans. on Robotics*, Vol. 24, No. 6, pp. 1289–1301, Dec. 2008.
6. H. Dong, M. Zhao and N. Zhang, "High-speed and energy-efficient biped locomotion based on virtual slope walking," *Autonomous Robots*, Vol. 30, No. 2, pp. 199–216, Feb. 2011.
7. T. Hayashi, K. Kaneko, F. Asano and Z.-W. Luo, "Experimental study of dynamic bipedal walking based on the principle of parametric excitation with counterweights," *Advanced Robotics*, Vol. 25, No. 1-2, pp. 273–287, Jan. 2011.
8. Y. Harata, F. Asano, K. Taji and Y. Uno, "Parametric excitation walking for four-linked bipedal robot," *Proc. of the 9th Int. IFAC Symp. on Robot Control*, pp. 589–594, Sept. 2009.
9. F. Asano and Z.-W. Luo, "Asymptotically stable biped gait generation based on stability principle of rimless wheel," *Robotica*, Vol. 27, Issue 6, pp. 949–958, Oct. 2009.
10. M. Garcia, A. Chatterjee, A. Ruina and M. Coleman, "The simplest walking model: Stability, complexity, and scaling," *J. of Biomechanical Engineering*, Vol. 120, Issue 2, pp. 281–288, April 1998.
11. F. Asano and Z.-W. Luo, "Efficient dynamic bipedal walking using effects of semicircular feet," *Robotica*, Vol. 29, Issue 3, pp. 351–365, May 2011.
12. F. Asano and M. Suguro, "Limit cycle walking, running, and skipping of telescopic-legged rimless wheel," *Robotica*, Vol. 30, Issue 6, pp. 989–1003, Oct. 2012.
13. J. Perry, Gait analysis: Normal and pathological function, SLACK Inc., 1992.